NDT&E International 60 (2013) 52–61

Contents lists available at ScienceDirect

NDT&E International

journal homepage: www.elsevier.com/locate/ndteint

Metal defects sizing and detection under thick coating using microwave NDT

Hong Zhang [a,1], Bin Gao [b,*,1], Gui Yun Tian [a,b], Wai Lok Woo [a], Libing Bai [b]

[a] School of Electrical, Electronic Engineering, Merz Court, Newcastle University, Newcastle Upon Tyne, NE1 7RU, United Kingdom
[b] School of Automation Engineering, University of Electronic Science and Technology of China, Chengdu, Sichuan 611731, China

ARTICLE INFO

Article history:
Received 10 January 2013
Received in revised form
4 July 2013
Accepted 5 July 2013
Available online 21 July 2013

Keywords:
Microwave NDT
Open-ended waveguide
Defect detection
Thick coating
Principle component analysis

ABSTRACT

An experimental study to evaluate shapes and sizes of defect under thick coating by microwaves NDT is demonstrated. Specially fabricated thick fire protect coated steel panels with embedded defects are inspected using an X-band (8.2–12.4 GHz) open-ended rectangular waveguide. The fundamental idea behind using this probe is presented along with several experimental results to validate this method for defect detection under coating. The reflected signal related to the phase and magnitude of the reflection coefficient at the waveguide aperture is used to create images of these coated samples under test. These images indicate the ability of microwaves for identifying and sizing defects under thick coating layer. Linear sweep technique is used here to obtain multiple frequency spectrum variances. Principle Component Analysis (PCA) algorithms have been employed to enhance the resolution of our proposed method. A series of performance comparison with PCA algorithms are also provided to extract the defect features from thick coating layer influence. To evaluate the proposed technique, steel with known defect and five coated steel plates with unknown defect under different coating thickness are measured. Results indicate that the defect detection capability has been enhanced with the suitable use of signal processing methods.

1. Introduction

Metal surface defect detection is very important in many industry areas (such as aircraft fuselage, nuclear power plant steam generator tubing and steel bridges etc.). Currently, there are several prominent non-destructive testing and evaluation (NDT & E) techniques for detecting surface defects on metals. Acoustic emission testing [1–3], eddy current [4,5], pulsed eddy current testing [6–9], eddy current thermography [10–12], ultrasonic testing [13,14], radiographic testing [15,16] and magnetic flux leakage testing [17–19] are examples of these techniques. Eddy current is widely using for surface defect detection. It can examine large areas very quickly and do not require use of coupling liquids. However, they have some crucial limitations: Eddy current and pulsed eddy current based NDT methods limited to be used in electrically conducting materials; the surface must be accessible and cannot detect defects with large lift-off (e.g. thick coating). Ultrasonic inspection is limited by high attenuation in the material while absorption for X-rays is too low for defects (harmful electromagnetic radiation). For the magnetic flux leakage, it can be used only for alloy and ferromagnetic materials.

With developments in materials science, lighter, stronger, and more durable dielectric materials are replacing or coating with metals in many applications. These materials require alternative testing approaches since traditional NDT methods may not be able to inspect them [20–22]. This is partly due to the relatively thick nature of these materials, attenuation and scattering caused by the various layers, low electrical conductivity associated with the layers, and thin planar anomalies that commonly appear in these structures. On the other hand, microwave NDT techniques are well suited for testing these structures since microwaves have a low absorption in dielectric materials, but they still strongly interacting to respond to structures and defects under these materials. In some situations (such as high temperature application), microwave NDT techniques may be the unique solution. For materials $\epsilon''/\epsilon' < 0.1$, penetration depth of microwave δ_d which depends on the operation frequency and the complex permittivity $\epsilon = \epsilon' + i\epsilon''$:

$$\delta_d = \frac{\lambda\sqrt{\epsilon'}}{2\epsilon''} \quad (1)$$

where λ is the wavelength and it depends on the operation frequency [23]. The penetration depth is calculated according to Eq. (1), which shows how it depends on the dielectric properties of the material. The penetration depth is used to denote the depth at which the power density has decreased to $(1/e)^2$ of its initial value at the surface.

* Corresponding author.
E-mail address: bingao831210@gmail.com (B. Gao).
[1] These authors have contributed equally.

0963-8695/$ - see front matter © 2013 Elsevier Ltd. All rights reserved.
http://dx.doi.org/10.1016/j.ndteint.2013.07.002

Materials with higher loss factor ϵ'' (imaginary part of the complex permittivity) show faster microwave energy absorption.

In the last two decades, researchers have shown interest in microwave NDT methods, because of the certain advantages of these methods such as remote detection, detection of filled and covered defects, estimating the physical dimension and orientation of the defects, and ease of operation [24–28]. Near-field open-ended waveguide microwave NDT technique appears to be one of the most promising techniques in detecting the presence or absence of a certain layer within layered structures [29]. With this method, the metal surface is scanned by an open-ended waveguide while its standing-wave characteristics are monitored. The defect detection and sizing with this method is prepared by analysing the overall reflection coefficient of the incident electric field at different defect positions beneath the open-ended waveguide aperture. This rectangular waveguide method must use a relatively high frequency in order to detect smaller defects, and this is because of the rectangular waveguide to detect only use primary molding [30,31]. Furthermore, in other applications, optimization of the measurement parameters, such as the frequency of operation, has shown measurement sensitivity to thickness variations in the range of a few micro-meters at frequencies in the X-band frequency range [32]. From signal processing point of view, many works have been already performed for spectral estimation and image reconstruction including but not limited to Fourier-based, correlation based, and super-resolution methods [33,34]. In the literature, spectral estimation or image reconstruction for samples under test has been limited to interpolation [35] in Fourier-based methods [36] and Inverse Fast Fourier Transform (IFFT) [37]. In addition, these methods only manually or use some criteria to select specific frequency band for analysis of defect, therefore, it lacks of deeply mining the informative from the whole band.

This paper presents the design and experimental testing of an open-ended waveguide operating in the X-band (8.2–12.4 GHz) for detecting defects on metal under thick coating layer. The sample under test is illuminated with electromagnetic waves. Then, a part of this incident wave will be absorbed in the coating layer, and another part will be transmitted and propagated through the coating layer. When it reached the metal layer, it will be total reflected. These forward and backward traveling waves inside the coating layer can be formulated by enforcing the appropriate boundary conditions at the air-coating and coating-conductor boundaries. The characteristics of the recorded reflected signal are utilized for detection and sizing of defects for the specimen under test. The reflection coefficient (which is the ratio of the reflected and transmitted waves) [27] from the waveguide aperture is monitored and recorded by a vector network analyser (VNA). Then this measurement data is used to produce imaging of sample under test. A C-scan system is designed for good sensitivity, penetration depth, and spatial resolution for defects evaluation under different coating thickness. A series of measurements was conducted to test the performance of this system.

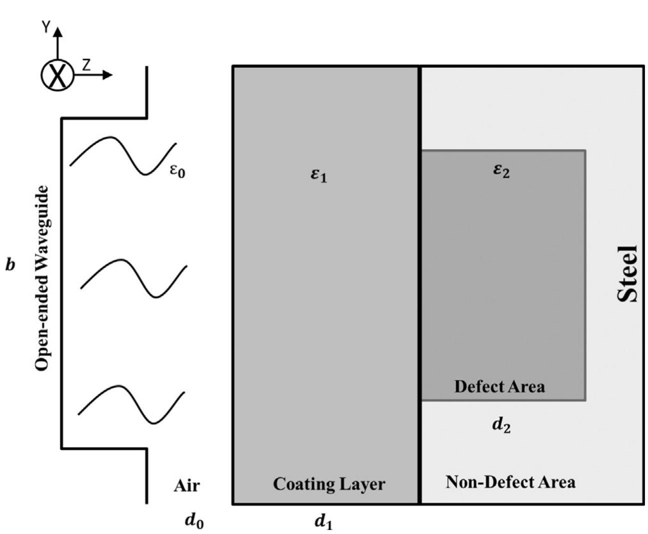

Fig. 1. Electromagnetic wave reflection and transmission for coated metal under test.

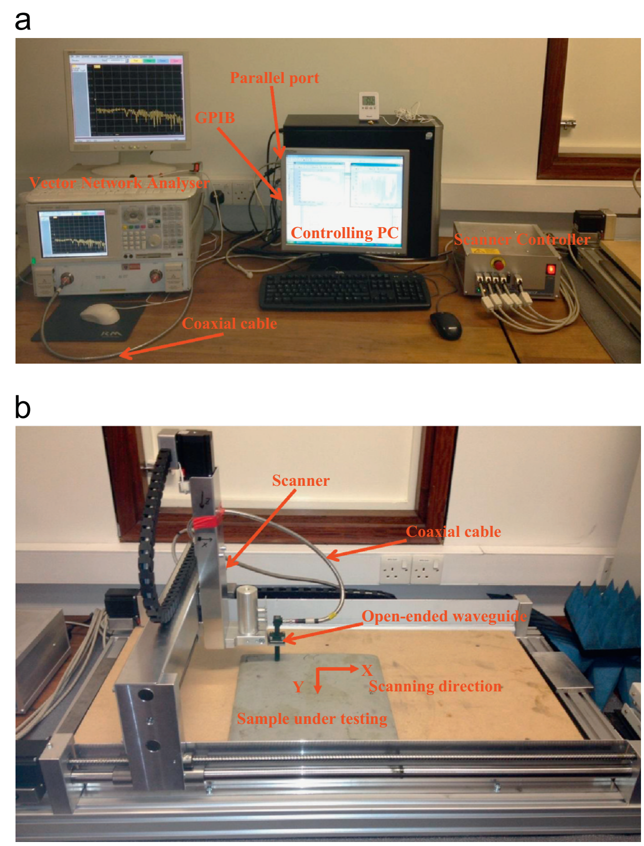

Fig. 2. Open-ended waveguide microwave NDT system experiment setup. (a) Controlling and signal processing platform and (b) Scanning platform.

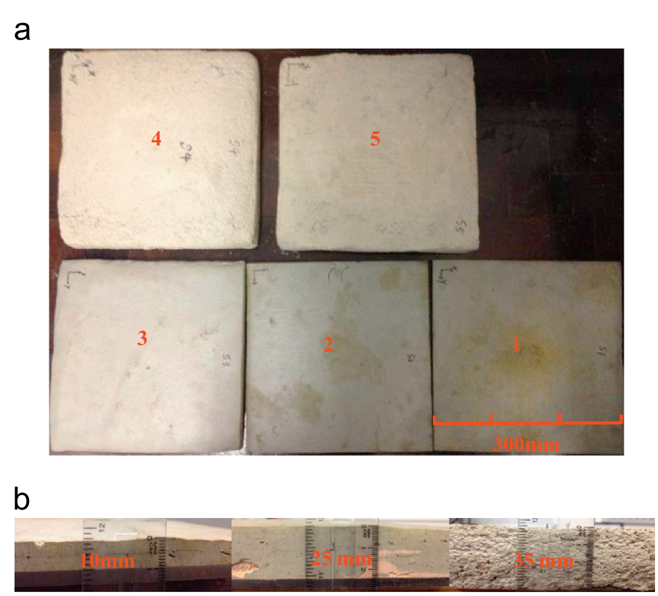

Fig. 3. Schematic of steel samples under test. (a) Coated steel samples for testing and (b) Coating layer thickness.

Table 1
Testing setup parameters for microwave NDT.

Parameter	Value
Sampling frequency range	8.2–12.4 GHz
Number of points for linear swept	201
Waveguide *x*–*y* dimensions (*a* × *b*)	22.86 mm × 10.16 mm
Scanning setup for steel sample with one hole under cement coating	$Lx=Ly=100$ mm Scanning step $\Delta x=\Delta y=2$ mm Diameter of hole $R=19$ mm Coating thickness 15 mm
Scanning setup for coated samples (Sample:1–5)	$Lx=Ly=280$ mm Scanning step $\Delta x=\Delta y=2$ mm
Thickness of coating layer (from left to right: Sample 1–5)	10 mm, 10 mm, 25 mm, 35 mm, 35 mm

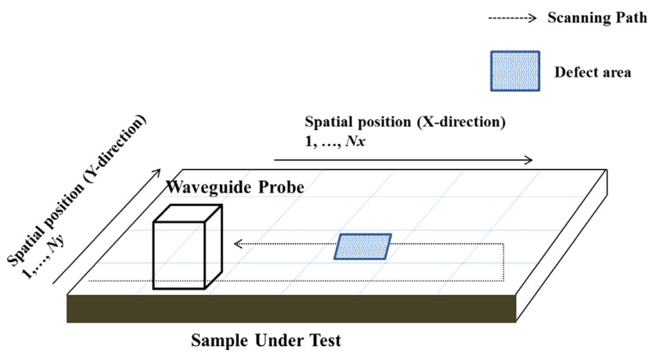

Fig. 4. Microwave NDT C-scan progress.

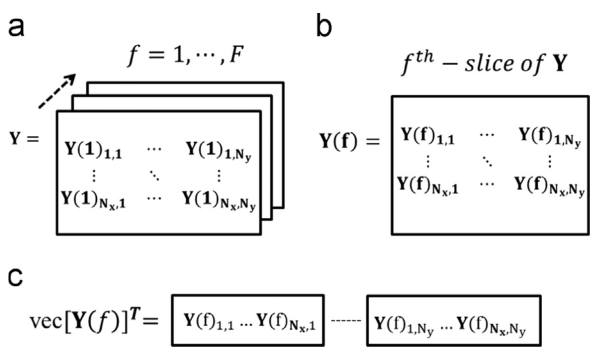

Fig. 5. (a) Tensor representation of the image sequences **Y**, (b) fth frame of **Y**, (c) visual explanation of vec($\mathbf{Y}(f)$)$^{\mathbf{T}}$.

This paper begins a brief overview of microwave NDT methods. The rest of this paper is divided into five parts. The first part deals with theoretical approach. Experiment system setup is given in the second part. A new approach of defect classification and characterisation based on Principal component analysis (PCA) is presented to extract the defect features from thick coating in the third part. Experiments results and discussions are provided in the fourth part. Finally, conclusions and further work are given.

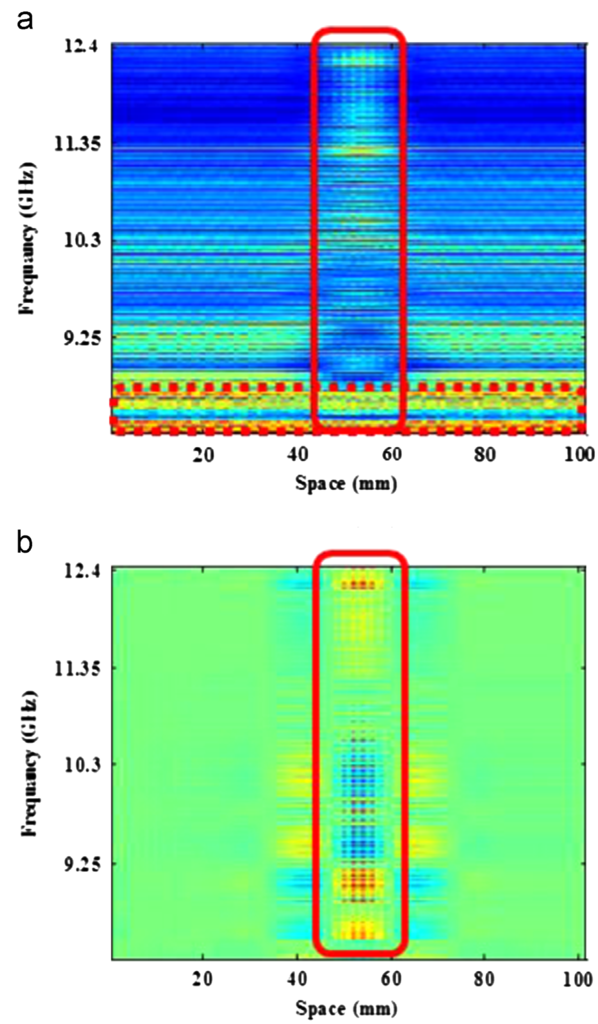

Fig. 6. (a) The amplitude spatial-frequency spectrum of steel sample with hole under test and (b) the amplitude spatial-frequency spectrum of steel with hole under test after PCA.

2. Theoretical approach

The problem of transmission and reflection of microwaves from a multilayer dielectric medium has been investigated by many investigators [38]. The following equations described here, are inspired from the model presented by Sayar, Seo and Ogawa [39]. A waveguide probe with dominant mode excitation (TE_{10}) is used to illuminate the structure with electromagnetic waves at microwave frequencies. The waveguide aperture lies in the x–y plane. Fig. 1 illustrates a sample consisting of coating layer and backed with a steel plate. This plane electromagnetic wave is linearly polarized. An incident signal is irradiated by the near-field of an open-ended waveguide. It is transmitted into the layered medium (coating and steel layers) and once reflected by the conducting plate. The ratio of these two signals gives the effective reflection coefficient of the sample under testing. Referring to Fig. 1, a generally lossy and homogeneous dielectric layer of relative permittivity ϵ_r and thickness d_1 is backed by a conducting substrate and is irradiated. A defect of

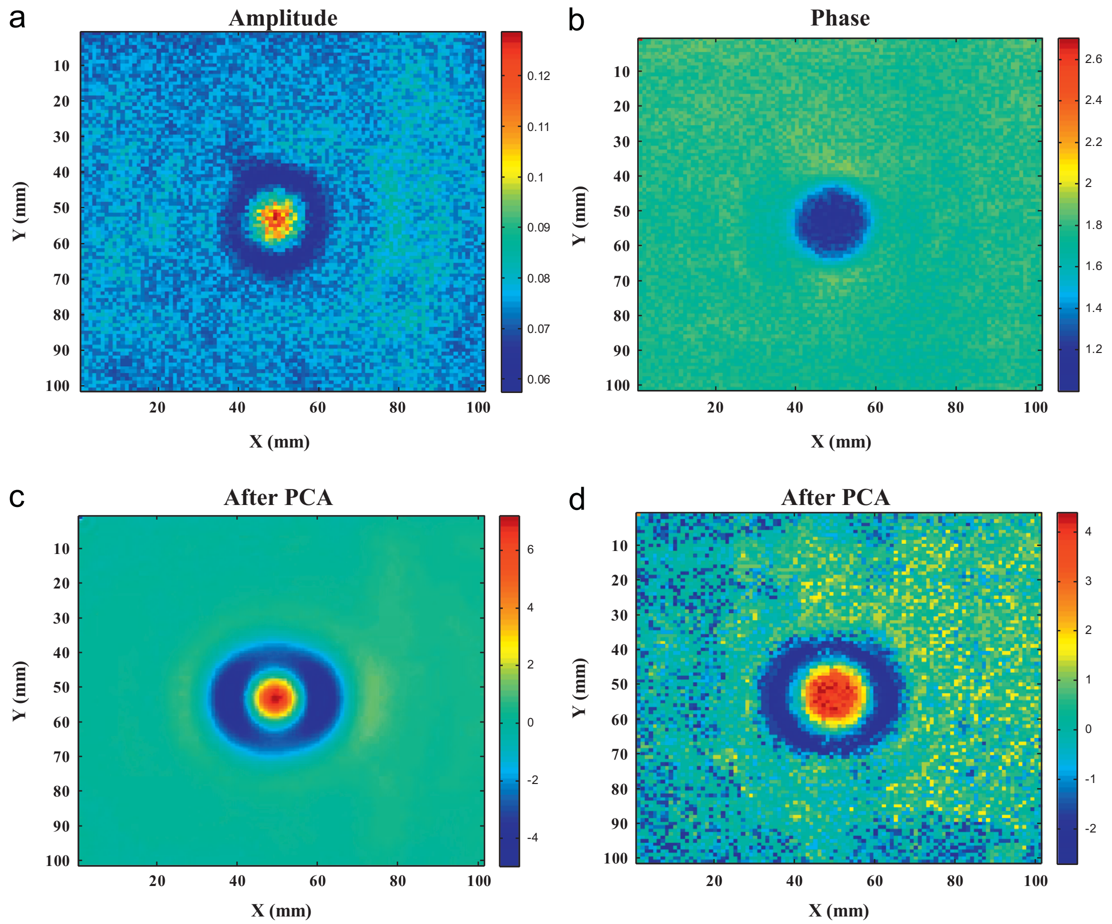

Fig. 7. Scan of steel with hole area (a) Amplitude variance (b) Phase variance at 12.4 GHz using X-band waveguide. With linear swept with X-band frequency range 2D images of defect can be obtained (c) Amplitude after PCA and (d) Phase after PCA.

certain thickness d_2 may be present in between the dielectric coating layer and the conducting steel layer.

The magnitude and phase difference between the reflection coefficients for non-coating and coating samples is related to the layer thickness and the permittivity (ϵ) of the sample under test. The lift-off d_0 here is known as the distance between waveguide and sample surface. Specifically, there should be a small air gap (non-contact) between the probe and the sample surface to have a smooth, simple movement of the waveguide. The propagation constant is represented the change of the electromagnetic wave as it propagates in a given direction. It is a complex quantity and can be written as: $\gamma=\alpha+i\beta$, where α, the real part, is called the attenuation constant, another symbol β, is actually the imaginary part, which represents the phase constant. Because the samples used in paper have no defect in the coating layer and the thickness of coating layer is almost same in each sample, therefore, the attenuation is approximately the same for each sample and can be considered as constant. For defect detection, when there is defect on the steel layer, the attenuation and reflection signal is significant differences between defect area and non-defect area due to the defect. The characteristics of the difference in recorded reflected signal are utilized for detection and sizing of defects for the specimen under test.

Calculation of the reflection coefficient for such a multiple mediums involves the derivation of the forward and backward travelling electric and magnetic field components in each layer based on a known incident field and the application of appropriate boundary conditions at each interface. The broad and narrow transverse dimensions of the waveguide are represented by a and b. Hence, for TE_{10} mode, the excitation aperture field distribution is given by

$$E_y(x,y,0)=\begin{cases}\sqrt{\frac{2}{ab}}\cos\left(\frac{\pi x}{a}\right), & (x,y)\in\text{aperture}\\ 0, & (x,y)\notin\text{aperture}\end{cases} \tag{2}$$

The complete set solutions for the field components for near-field open-ended waveguide NDT is constructed by Bakhtiari et al. [40]. Variational expression for the admittance of the waveguide can be written as

$$y_s=\frac{j}{(2\pi)^2\sqrt{1-\left(\frac{\lambda_0}{2a}\right)^2}}\int_{R=0}^{\infty}\int_{\theta=0}^{2\pi}\mathcal{J}\left\{(K^2-R^2\cos^2\theta)\left(2C_\phi+\frac{j\mathcal{J}}{X_z}\right)\right\}R\,d\theta\,dR \tag{3}$$

$$\mathcal{J}=\sqrt{\frac{2A}{B}}\frac{4\pi\sin\left(\frac{X_yB}{2}\right)\cos\left(\frac{X_xA}{2}\right)}{X_y[\pi^2-(X_xA)^2]} \tag{4}$$

$$C_\phi=-\frac{\mathcal{J}e^{jX_zD}}{2X_z\sin(X_zD)} \tag{5}$$

$$A=k_0a,\ B=k_0b,\ D_{\text{non-defect}}=k_0(d_0+d_1)\ \text{or}\ D_{\text{defect}}=k_0(d_0+d_1+d_2) \tag{6}$$

$$K=\frac{k_1}{k_0},\ X_x=R\cos\theta,\ X_y=R\sin\theta,\ X_z=\sqrt{K^2-R^2} \tag{7}$$

where R and θ are the new variables of integration in polar coordinates. The complex reflection coefficient, Γ is related to complex admittance, y_s, by

$$\Gamma = \frac{1-y_s}{1+y_s} \tag{8}$$

From above equations, the reflection coefficient is different when there is defect on the steel sample. Both amplitude and phase of reflection coefficient can be used for defect detection. Macroscopically, when there is a defect under these coated metal samples, they exhibit surface discontinuities. Due to the nature physical properties difference, these discontinuities affect through the microwave changes in attenuation and absorption in metal. Therefore, the defect information (such as size and location etc.) can be deduced from the received reflection signals. These reflected signals is measured and then used to calculate reflection coefficient by VNA. These complex reflection coefficients are complex number whose phase and magnitude which refers to frequency spectrum variations. This measurement data will provides information about location and dimensions of the defect [41]. This is a very sensitive interaction and is function of defect dimensions and placement within the waveguide aperture.

3. Experiment setup

The experimental set-up is shown in Fig. 2. An X-band (from 8.2 GHz to 12.4 GHz) open-ended rectangular waveguide is mounted with an X-Y scanner. This probe is a standard WR-90 waveguide with the aperture dimensions of 22.86 mm × 10.16 mm and the flange dimensions are 42.2 mm × 42.2 mm. The sample is placing under the waveguide with a certain lift-off. A vector network analyser (Agilent PNA E8363B) is employed here to provide signal source and obtain the frequency spectrum information of the reflected signal. The waveguide is connected with the vector network analyser through a coaxial cable. A control PC here is used to control and acquire the measurement data from vector network analyser through IEEE-488 GPIB (General Purpose Interface Bus). The X–Y scanner is controlled by X–Y scanner controller. This controller is connected with the parallel port of the control PC. A MATLAB program is designed and used to controlling vector network analyser and X–Y scanner.

During the measurement, the frequency range is set from 8.2 GHz to 12.4 GHz. A linear sweep is applied over this frequency range (frequency resolution is about 0.02 GHz with 201 linear sweep points). This whole reflected frequency spectrum is obtained by using linear sweep frequency technology with vector network analyser (the vector network analyser measures reflection coefficient for each operation frequency over whole sweep frequency range). Lift-off is set as 1.5 mm. At each measurement location in this space, the waveguide is used to illuminate the sample under test and receive the reflected signal, whose magnitude and phase are detected and recorded. These recorded measurements, corresponding to the 2-D scanning space, are subsequently processed to produce an image of the sample under test.

Five coated steel samples (width is 300 mm, length is 300 mm, thickness of steel plate is 5 mm, thickness of coating is different) with man-made defects are measured with proposed Microwave NDT method. This steel sample has one hole (19 mm diameter for comparison study), five steel samples (Fig. 3 shows the schematic of these steel samples under test.). The experiments architecture of microwave detection system based on rectangular waveguide probe (a is broad dimension of the open-ended rectangular waveguide aperture, b is narrow dimension of the open-ended rectangular waveguide aperture). The measurement conditions used to develop the following results are listed in Table 1.

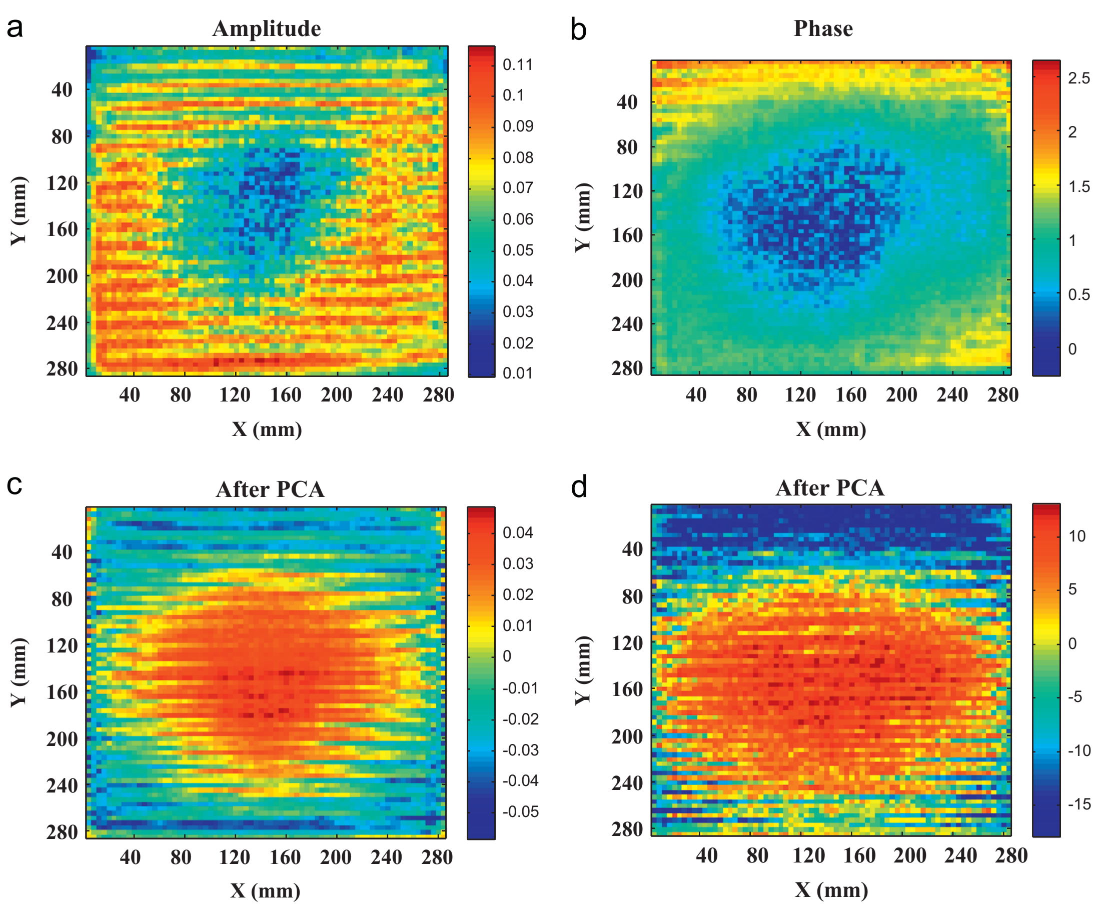

Fig. 8. Scan of steel with 15 mm paint (a) Amplitude variance (b) Phase variance at 12.4 GHz using X-band waveguide. With linear swept with X-band frequency range 2D images of defect can be obtained (c) Amplitude after PCA and (d) Phase after PCA.

4. Defect characterisation with PCA

A raster-like relative motion of waveguide probe with respect to the sample gives a data set that can be visualized as an image.

The observation of Fig. 4 can be considered as the tensor representation of mixing spatial-frequency spectrum observation $\mathbf{Y}$ which is the combination of non-defect and defect spatial-frequency spectrum sources, respectively [42,43]. In $\mathbf{Y}$, the frequencies are given by $f=1,2,\ldots,F$ and F represents the total frequency units. The tensor observation can be expanded in matrix format as $\mathbf{Y}'=[\mathrm{vec}(\mathbf{Y}(1)),\mathrm{vec}(\mathbf{Y}(2)),\ldots,\mathrm{vec}(\mathbf{Y}(F))]^{\mathbf{T}}$ where $\mathbf{Y}(f)$ denotes the spatial-frequency spectrum matrix with dimension $N_x\times N_y$ of the fth slice of $\mathbf{Y}$. The visual explanation of this tensor flattening process is given in Fig. 5.

In this paper, both magnitude $\mathbf{Y}_M^{'}=|\mathbf{Y}'|$ and phase $Y'_P=atan(Im(Y')/Re(Y'))$ information of $\mathbf{Y}'$ are used for processing and analysis to produce defect images. As sweep frequency technique is used during the testing, multiple operation frequencies have been applied. For further comparison study, one operation frequency 12.4 GHz is used to provide 2D defect images with amplitude and phase. In order to enhance the resolution of defect image, the principal component analysis (PCA) is used. For those PCA results, the whole X-band frequency range (8.2 GHz to 12.4 GHz) is using to extract the defects information under coating.

Principal component analysis (PCA) is extensively used in feature extraction to reduce the dimensionality of the original data by a linear transformation. PCA extracts dominant features from a set of multivariate data. The dominant features retain most of the information, both in the sense of maximum variance of the features and in the sense of minimum reconstruction error. PCA is used to extract the defect information from coating layer surface roughness and thick layer attenuation. The obtained signal contains three uncorrelated source signals: one comes from the surface of coating layer, one from the coating layer and the third one are from the metal surface. As the microwave signal is total reflected by the metal, the third signal is stronger than the other two. However with relative small defects, this signal may be covered by the other two. PCA is used here to extract defect source from the received signals. We take $\mathbf{Y}'_M$ as an example of using PCA (the $\mathbf{Y}_P^{'}$ can be processed by using the same step), the $\mathbf{Y}'_M$ can be transformed into uncorrelated sources by means of a whitening matrix based on the eigenvalue decomposition (EVD) of the covariance matrix $E\{\mathbf{Y}_M^{'}\mathbf{Y}_M^{'\mathbf{T}}\}=\mathbf{EDE}^{\mathbf{T}}$, where $\mathbf{E}$ is the orthogonal matrix of eigenvectors and $\mathbf{D}=\mathrm{diag}(\lambda_1,\ldots\lambda_N)$, being $\lambda_1\geq\ldots\geq\lambda_N$ the eigenvalues. After using PCA to obtain the uncorrelated sources, it is also possible to reduce the transformed output dimension, e.g. by choosing $N_s\leq N$, there exists N_s number of uncorrelated sources with maximally informative subspace of input data $\mathbf{Y}'_M$. In this paper, we have plotted both raw data and PCA results. The plot has concretely shown that the resolution of defect image can be improved by using the PCA.

To validate our proposed method, one steel sample with a known hole is covered with 15 mm cement layer. Results for this steel with hole are presented below:

To understand different microwave spectrum property for NDE, linear sweep frequency technology has been employed. Fig. 6 shows the line scanning results through centre of steel sample with hole under swept frequencies, the defect area is been highlighted by the solid line in both figures. The magnitude of the reflection coefficient is used to create images of defects. As shown in Fig. 6, with linear sweep frequency technique, the frequency spectrum has been obtained. With higher operation frequencies,

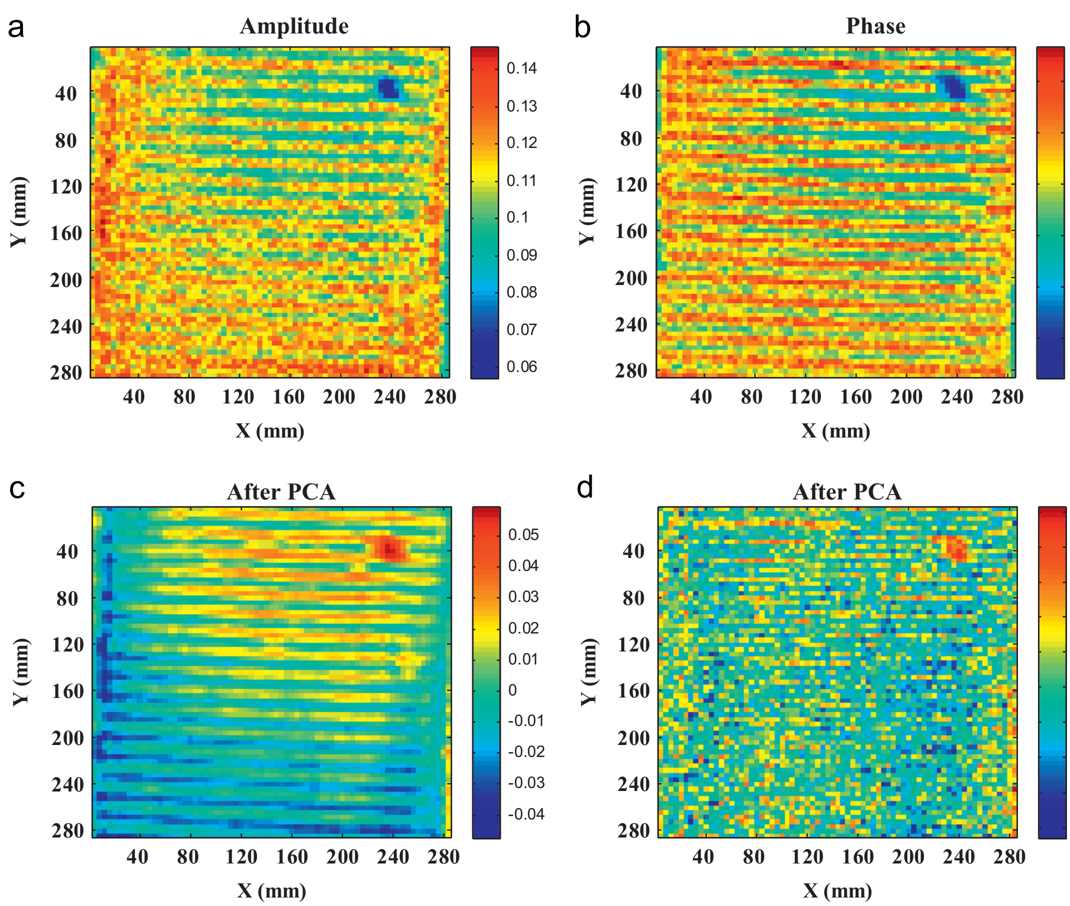

Fig. 9. Scan of steel with 15 mm paint (a) Amplitude variance (b) Phase variance at 12.4 GHz using X-band waveguide. With linear swept with X-band frequency range 2D images of defect can be obtained (c) Amplitude after PCA and (d) Phase after PCA.

the hole can be easily detected. However, at the lower frequency range (less than 9 GHz as dot line shown in Fig. 6(a)), it is hard to detect the hole. After PCA processing (Fig. 6(b)), the influence of roughness and thick coating has been largely eliminated, the results have been enhanced compare to original results (as solid line shown in both Fig. 6(a) and (b)).

It can be seen from Fig. 7, the hole can be detected by using both amplitude and phase of reflection coefficient. When the probe encounters the opening of a defect, the reflection coefficient is changed (as it can be seen in Eqs. (2) and (7)), indicating the existence of a defect within the probe aperture. This feature can be used to determine the defect size. In fact, when the scan direction is normal to the defect lips, the probe observes a non-short-circuit reflection coefficient for a distance $b+R$, where the received signal is not constant (where b is narrow dimension of the open-ended rectangular waveguide aperture, R is diameter of the hole on the steel sample). During our measurement, the scanning direction is moving with the dimension of the open-ended rectangular waveguide aperture. The obtained size of defect is around 30 mm by 30 mm (obtained defect diameter $b+R=10.16+19=29.16$ mm). Error variances between estimated values and real values are less than 2.8% which is quite accurate.

Due to the coating surface is not smooth, as the phase has more influence with the coating thickness variance (attenuation of coating layer is different with thickness variance), both amplitude and phase can be used for defect detection under thick coating (it can be seen from Fig. 7(a) and (b)). As can be seen, the presence of the hole can be easily obtained, and it produces a distinct image associated with this hole. As shown in the figures, one red spot surrounded by partial circular rings represent the presence of the hole. It is assumed that these rings correspond to the edges of the hole, and the spacing of which may increase or decrease as a function of the hole diameter, the frequency of operation and the transition aperture dimensions. The rings are not complete circles because of the linear polarization and aperture dimensions of the waveguide. As can be seen, the signal produced, including the rings, is larger than the physical size of the hole. This is advantageous since the scans produce a signal due of hole which is larger than the physical size of the hole (when this hole is too small to detect, with this method, this hole could be detected). Because the reflected signal from non-defect areas share the similarity of spectrum characteristics, and these spectrum characteristics are different from the one from defect area and can be assumed they are uncorrelated. With employing PCA, it separates the input signal into uncorrelated subspace. In each subspace, the signal share similar features. Thus, most of reflected signals from non-defect areas have been captured in one PC subspace. On the other hand, the reflected signals from defect areas have been captured in another PC subspace; therefore, the defect areas can be separated and the resolution of defect detection results can be enhanced. More accurate and clear results can be obtained (it can be seen from Fig. 7(c) and (d)).

5. Experiments results and interpretations

Different experimental results and analysis for unknown Defects and Feature Extraction with PCA are discussed below.

Results for sample 1 are show in Fig. 8.

As we can see from Fig. 8, both amplitude and phase can be used for defect detection under thick paint (15 mm). The sample 1 is punched by a hammer. With 12.4 GHz inspection frequency, the defect is been detected and located, but the size

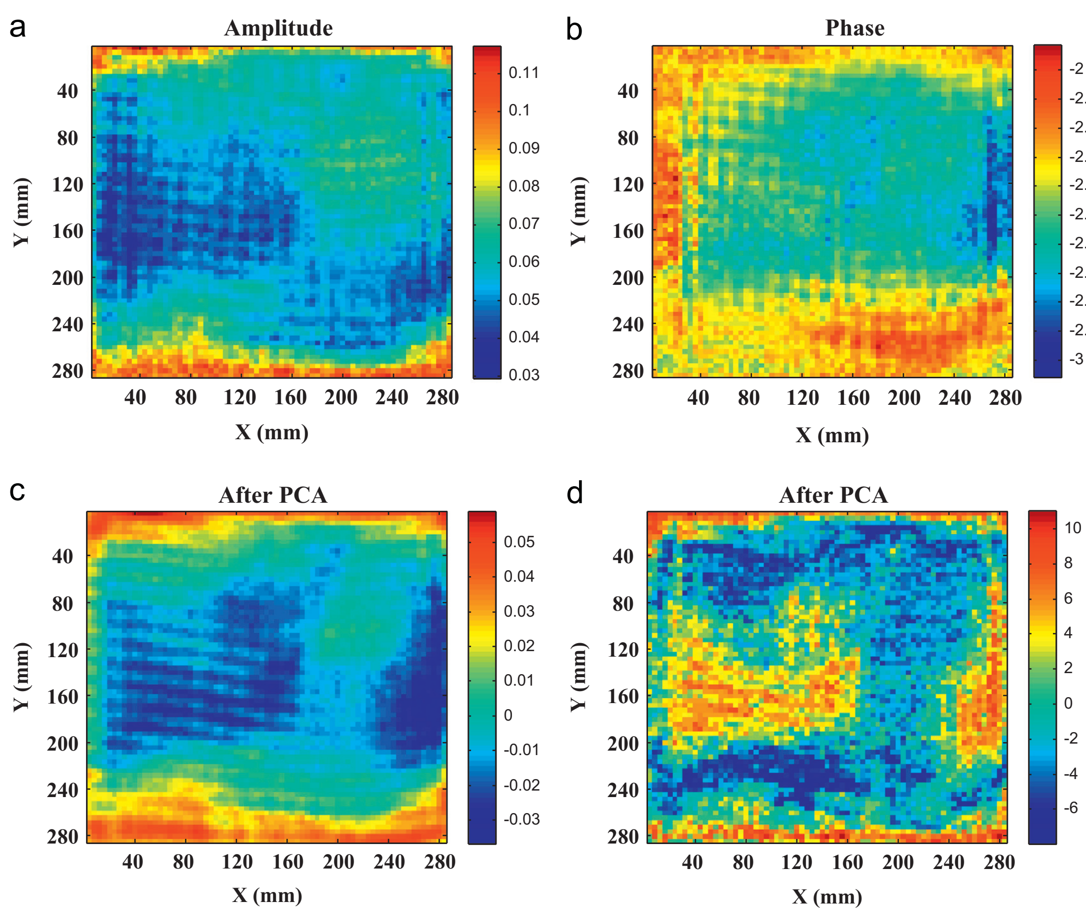

Fig. 10. Scan of steel with 25 mm paint (a) Amplitude variance (b) Phase variance at 12.4 GHz using X-band waveguide. With linear swept with X-band frequency range 2D images of defect can be obtained (c) Amplitude after PCA and (d) Phase after PCA.

is not very clearly comparing amplitude results with phase results. With linear sweep frequency technique, applied PCA, confines and location of defect are been obtained. It can be seen from Fig. 8(c) and (d), the phase suffering more influence from the coating layer variance. For size estimation, the amplitude is more suitable than phase. The obtained size of defect area is around 118 mm by 110 mm.

Results for sample 2 are shown in Fig. 9.

From Fig. 9, one small defect has been obtained under paint (15 mm) in the sample 2. The position of defect has been located. With only one operation frequency employed, the location of this defect has been identified. Comparison Fig. 9 (a) with (b), it is much easier obtaining the defect with amplitude rather than that of phase. But it is still very difficult to estimate the size of defect. After applied PCA with whole X-band frequency, both amplitude and phase can be used to estimate the size of the defect (it can be seen from Fig. 9(c) and (d)) which diameter is around 20 mm.

Results for sample 3 are shown in Fig. 10.

From Fig. 10, the experiment results can be obtained for the sample 3. The paint thickness is around 25 mm. It can be seen from Fig. 10, with one operation frequency, it is very difficult to locate and identify these defects. Due to thick coating layer and complex geometry structure influence, defect areas are hard to obtain. After applied PCA, this influence of coating layer has been separated. Two defect areas have been obtained and located in Fig. 10(c) and (d). The sizes of these two areas are 120 mm by 80 mm and 40 mm by 80 mm.

Results for sample 4 are shown in Fig. 11.

Sample 4 is a steel plate coated with concrete (40 mm thickness). It has been punched in the metal plate. For defect detection, the defect location and area can be obtained with phase when only employing one operation frequency (it can be seen from Fig. 12 (a) and (b)). The phase is more sensitive than amplitude. The punched area has been located and obtained after using PCA with amplitude and phase. The size is around 120 mm by 80 mm. More accurate results have been obtained from these images. Another important finding was that more accurate result has been obtained with amplitude after PCA. After the application of PCA, both amplitude and phase results have been enhanced. Shape of defect is obtained with our proposed method.

Results for sample 5 are shown in Fig. 12.

Sample 5 is coated with 40 mm concrete too. Compare the amplitude results with phase results, the amplitude have been suffering more influence from coating thickness variance and surface roughness. As can be seen Fig. 12(a) and (b), the defect area has been obtained with phase when only employing one operation frequency. From Fig. 12(c) and (d), the defect area has been obtained and located after applied PCA. Another important finding was that PCA separates the influence from coating layer. The shape and location of the defect are much clearer after applied PCA.

6. Conclusions and further work

The ability of microwaves to penetrate non-conductive material makes microwave techniques attractive to inspect the presence of defects and damage under un-metallic layers. In this paper, a novel Microwave NDT based system has been presented to solve the defect detection under thick coating issue. This system uses an

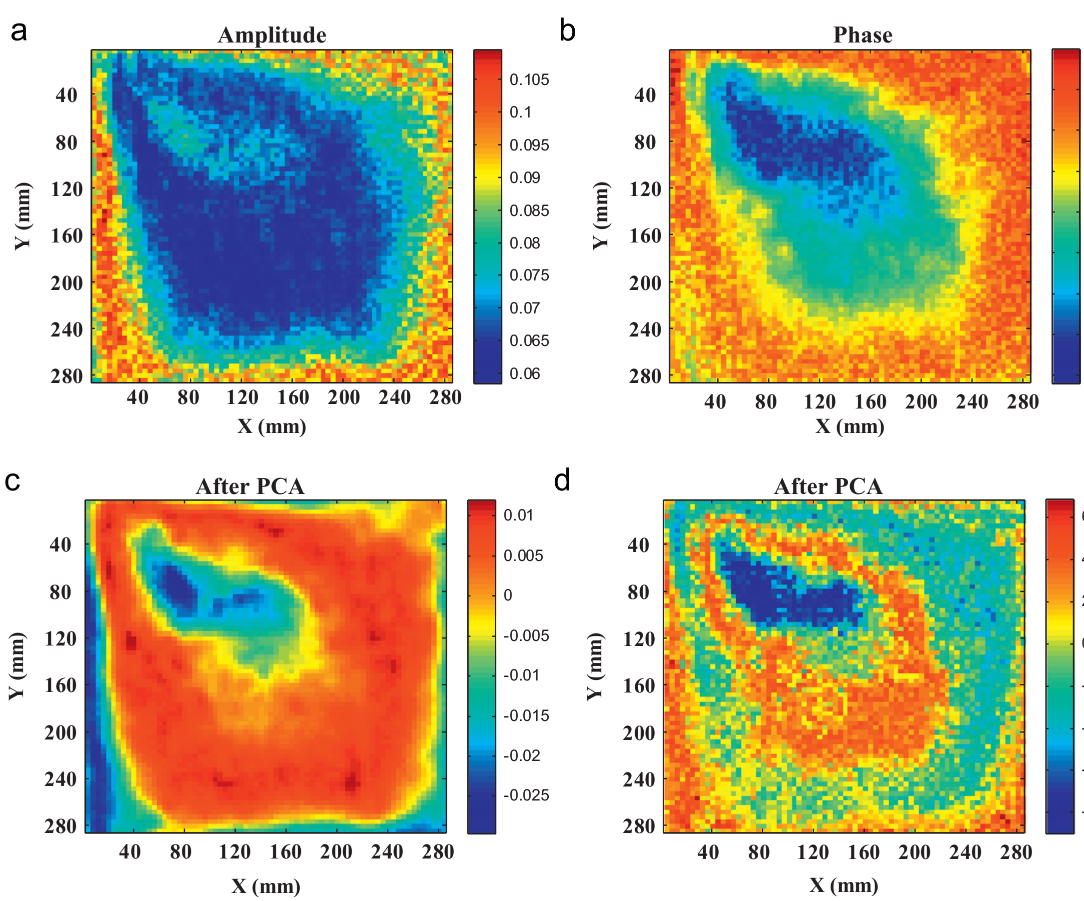

Fig. 11. Scan of steel with 40 mm paint (a) Amplitude variance (b) Phase variance at 12.4 GHz using X-band waveguide. With linear swept with X-band frequency range 2D images of defect can be obtained (c) Amplitude after PCA and (d) Phase after PCA.

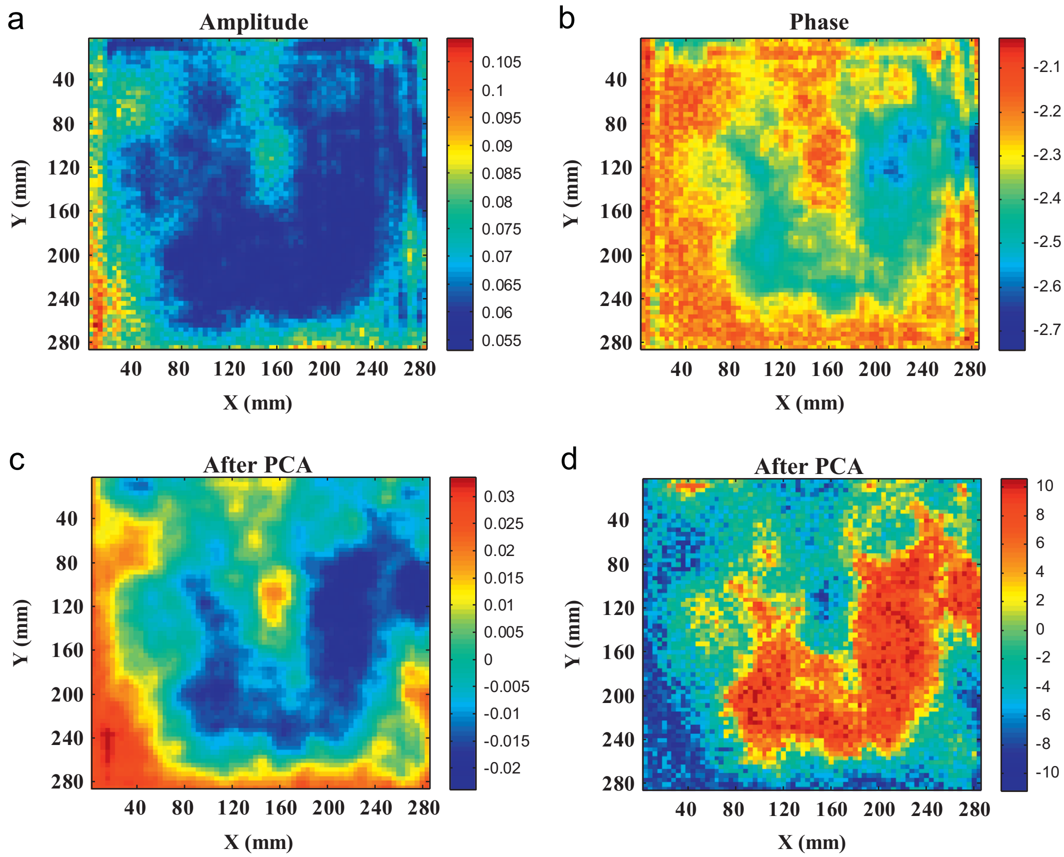

Fig. 12. Scan of steel with 40 mm paint (a) Amplitude variance (b) Phase variance at 12.4 GHz using X-band waveguide. With linear swept with X-band frequency range 2D images of defect can be obtained (c) Amplitude after PCA and (d) Phase after PCA.

X-band rectangular waveguide with a vector network analyser for non-destructive test application. The reflection coefficient at the waveguide aperture is used to create images of these defects. These images indicate the ability of microwaves for detecting and locating defects with different sizes and shapes in metal sample. Simple C-scans has revealed the potential of this technique as a tool to inspect the integrity of coated steel sample. Defect location has been demonstrated to be an easy task to achieve using our suggested technique. In addition to detecting and locating defects, thickness variations in the coating layer could be monitored using this technique in conjunction with phase information. A new approach of defect classification and characterisation based on linear sweep frequency and Principal Component Analysis (PCA) has been demonstrated. The PCA globally analyses across the whole X-band frequencies range and therefore avoid the interpolation issue faced by conventional Fourier-based methods. The linear sweep frequency technique with PCA largely eliminates the influence of roughness and thick coating.

Overall, the results are very encouraging. The use of near-field microwave techniques, utilizing open-ended rectangular waveguides, can be used to detect the presence of surface defect in metal under paint. The images generated from 2-D raster scans can show relative defect size and location. A further application may involve using this technique with advanced signal processing technology to reduce processing time.

Acknowledgement

The authors would like to thank International Paint for providing samples and FP7 funded HEMOW project 269202.

References

[1] Ivanov VI. Acoustic emission: some problems, tasks and solutions. NDT International 1984;17:323–8.
[2] Akhtar A, Wong JY, Bhuyan GS, Webster CT, Kung D, Gambone LR, et al. Acoustic emission testing of steel cylinders for the storage of natural gas on vehicles. NDT & E International 1992;25:115–25.
[3] Camerini CS, Rebello JMA, Soares SD. Relationship between acoustic emission and CTOD testing for a structural steel. NDT & E International 1992;25:127–33.
[4] Helifa B, Oulhadj A, Benbelghit A, Lefkaier IK, Boubenider F, Boutassouna D. Detection and measurement of surface cracks in ferromagnetic materials using eddy current testing. NDT and E International 2006;39:384–90.
[5] Song SJ, Shin YK. Eddy current flaw characterization in tubes by neural networks and finite element modeling. NDT and E International 2000;33:233–43.
[6] Tian GY, Sophian A. Defect classification using a new feature for pulsed eddy current sensors. NDT & E International 2005;38:77–82.
[7] Bai L, Tian GY, Simm A, Tian S, Cheng Y. Fast crack profile reconstruction using pulsed eddy current signals. NDT & E International 2013;54:37–44.
[8] He Y, Luo F, Pan M. Defect characterisation based on pulsed eddy current imaging technique. Sensors and Actuators, A: Physical 2010;164:1–7.
[9] He Y, Luo F, Pan M, Hu X, Liu B, Gao J. Defect edge identification with rectangular pulsed eddy current sensor based on transient response signals. NDT & E International 2010;43:409–15.
[10] Cheng L, Tian GY. Surface crack detection for carbon fiber reinforced plastic (CFRP) materials using pulsed eddy current thermography. IEEE Sensors Journal 2011;11:3261–8.
[11] Wilson J, Tian GY, Mukriz I, Almond D. PEC thermography for imaging multiple cracks from rolling contact fatigue. NDT and E International 2011;44:505–12.
[12] Pan M, He Y, Tian GY, Chen D, Luo F. Defect characterisation using pulsed eddy current thermography under transmission mode and NDT applications. NDT and E International 2012;52:28–36.
[13] Drinkwater BW, Wilcox PD. Ultrasonic arrays for non-destructive evaluation: a review. NDT and E International 2006;39:525–41.
[14] Cobb AC, Michaels JE, Michaels TE. An automated time-frequency approach for ultrasonic monitoring of fastener hole cracks. NDT and E International 2007;40:525–36.
[15] Nakamura K, Mukae S, Katoh M, Nishio K. Fundamental study of detectability of subsurface defects by radiographic testing: nondestructive testing and evaluation. NDT and E International 1998;31:222 (7 1–6, pp. 319–335 (1992).
[16] da Silva RR, Calôba LP, Siqueira MHS. Rebello JMA. Pattern recognition of weld defects detected by radiographic test. NDT & E International 2004;37:461–70.

[17] Li Y, Tian GY, Ward S. Numerical simulation on magnetic flux leakage evaluation at high speed. NDT and E International 2006;39:367–73.
[18] Li Y, Wilson J, Tian GY. Experiment and simulation study of 3D magnetic field sensing for magnetic flux leakage defect characterisation. NDT & E International 2007;40:179–84.
[19] Zhang Y, Ye Z, Wang C. A fast method for rectangular crack sizes reconstruction in magnetic flux leakage testing. NDT & E International 2009;42:369–75.
[20] Kharkovsky S, Zoughi R. Microwave and millimeter wave nondestructive testing and evaluation—overview and recent advances. IEEE Instrumentation and Measurement Magazine 2007;10:26–38.
[21] Microwave NDT: 51587 Ida, N. Kluwer, 394pp. (1992). NDT & E International.; 1994, 27:335.
[22] Review of NDT techniques at radio and microwave frequencies: 43328 Zoughi, R. Review of progress in quantitative nondestructive evaluation, vol. 8A. Edited by D.C. Thompson and D.E. Chimenti, pp. 337–344. Plenum Press (1989), ISBN 0 306 43209 9. NDT & E International.; 1994, 27:339.
[23] Troch PA, Vandersteene F, Su Z, Hoeben R, Wuethrich M. Estimating microwave observation depth in bare soil through multi-frequency scatterometry. In: First EMSL User Workshop Proceedings, Ispra, Italy1996.
[24] A novel technique for microwave thickness measurement of dielectric slabs using an open-ended rectangular waveguide: 51350 Bakhtiari, S.; Ganchev, S.; Zoughi, R. Review of progress in quantitative nondestructive evaluation, Brunswick, Maine (United States), 28 Jul.–Aug. 1991. Vol. 11A, pp. 529–535. Edited by D.O. Thompson and D.E. Chimenti. Plenum Press (1992). NDT & E International.; 1994. 27:335.
[25] Yeh CY, Ranu Y, Zoughi R. A novel microwave method for surface crack detection using higher order waveguide modes: 55289 materials evaluation. NDT and E International 1994;27:332.
[26] Mazlumi F, Sadeghi SHH, Moini R. Analysis technique for interaction of rectangular open-ended waveguides with surface cracks of arbitrary shape in metals. NDT & E International 2003;36:331–8.
[27] Sayar M, Seo D, Ogawa K. Non-destructive microwave detection of layer thickness in degraded thermal barrier coatings using K- and W-band frequency range. NDT & E International 2009;42:398–403.
[28] Mazlumi F, Gharanfeli N, Sadeghi SHH, Moini R. An open-ended substrate integrated waveguide probe for detection and sizing of surface cracks in metals. NDT & E International 2013;53:36–8.
[29] Qaddoumi NN, Saleh WM, Abou-Khousa M. Innovative near-field microwave nondestructive testing of corroded metallic structures utilizing open-ended rectangular waveguide probes. IEEE Transactions on Instrumentation and Measurement 2007;56:1961–6.
[30] Microwave imaging techniques for non-destructive testing of materials: 52890 Bolomey, J.C.; Pichot, C. Microwave processing of materials III, San Francisco, California (United States), Apr. 27–May 1. 1992. pp. 479–489. Edited by R.L. Beatty, W.H. Sutton and M.F. Iskander. MRS. 269 (1992). NDT & E International; 1994. 27:333.
[31] Surface microwave imaging for nondestructive evaluation of civil structures: 54637 D′Errico, M.S.; Douglas, B.L. Lee, L. 1993 IEEE International conference on acoustics, speech and signal processing, Minneapolis (United States), 27–30 Apr. 1993. p. V-453- V0456. IEEE vol. 5 (1993). NDT & E International; 1994. 27:332.
[32] Bakhtiari S, Ganchev SI, Zoughi R. Microwave swept-frequency optimization for accurate thickness or dielectric property monitoring of conductor-baked composites. Materials Evaluation 1993;51:740–3.
[33] DeGraaf SR. SAR imaging via modern 2-D spectral estimation methods. IEEE Transactions on Image Processing 1998;7:729–61.
[34] Barbarossa S, Marsili L, Mungari G. SAR super-resolution imaging by signal subspace projection techniques. AEU-Archiv fur Elektronik und Ubertragungstechnik 1996;50:133–8.
[35] Craig M. Analytic signals for multivariate data. Mathematical Geology 1996;28:315–29.
[36] Gröchenig K, Strohmer T. Numerical and theoretical aspects of nonuniform sampling of band-limited images. In: Marvasti F, editor. Nonuniform sampling. US: Springer; 2001. p. 283–324.
[37] Abbasi K, Ito S, Hashizume H. Prove the ability of microwave nondestructive method combined with signal processing to determine the position of a circumferential crack in pipes. International Journal of Applied Electromagnetics and Mechanics 2008;28:429–39.
[38] Zoughi R, Bakhtiari S. Microwave nondestructive detection and evaluation of disbonding and delamination in layered-dielectric slabs. IEEE Transactions on Instrumentation and Measurement 1990;39:1059–63.
[39] Sayar M, Seo D, Ogawa K. Non-destructive microwave detection of layer thickness in degraded thermal barrier coatings using K- and W-band frequency range. NDT and E International 2009;42:398–403.
[40] Bakhtiari S, Qaddoumi N, Ganchev SI, Zoughi R. Microwave noncontact examination of disbond and thickness variation in stratified composite media. IEEE Transactions on Microwave Theory and Techniques 1994;42:389–95.
[41] Zoughi R, Kharkovsky S. Microwave and millimetre wave sensors for crack detection. Fatigue and Fracture of Engineering Materials and Structures 2008;31:695–713.
[42] Bin Gao, Woo WL, Dlay SS. Single Channel Source Separation Using EMD-Subband Variable Regularized Sparse Features, *IEEE Transactions on Audio, Speech and Language Processing*, May 2011;19: 961–76.
[43] Libing Bai, Bin Gao, Gui Yun Tian, Yuhua Cheng. Spatial and Time Patterns Extraction of Eddy Current Pulsed Thermography using Blind Source Separation, *IEEE Sensors Journal*, 2013;13:2094–101.